Research Square

Preprints are preliminary reports that have not undergone peer review.
They should not be considered conclusive, used to inform clinical practice,
or referenced by the media as validated information.

Divergent systemic and airway mucosal adaptive immunity to SARS-CoV-2 in African adults

Gloria Kapira

gkapira@mlw.mw

Malawi-Liverpool Wellcome Research Programme https://orcid.org/0009-0000-4489-8287

Joseph Phiri

Malawi-Liverpool Wellcome Research Programme

Robert Nyirenda

Malawi-Liverpool Wellcome Research Programme

Memory Mvula

Malawi-Liverpool Wellcome Research Programme

Edwin Lisimba

Malawi-Liverpool Wellcome Research Programme

Austine Kumwenda

Malawi-Liverpool Wellcome Research Programme

Dorothy Kazembe

Malawi-Liverpool Wellcome Research Programme

Alice Kusakala

Malawi-Liverpool Wellcome Research Programme

Anstead Kankwatira

Malawi-Liverpool Wellcome Trust Clinical Research Programme

Rose Malamba

Malawi-Liverpool Wellcome Trust Clinical Research Programme

Lucy Cooper

University College London

Mariana Diniz

UCL

Elena Mitsi

Oxford University https://orcid.org/0000-0001-7586-6050

Mala Maini

UCL https://orcid.org/0000-0001-6384-1462

Daniela Ferreira

Oxford University https://orcid.org/0000-0002-0594-0902

Rhona Mijumbi

Malawi-Liverpool Wellcome Research Programme

Henry Mwandumba

Malawi Liverpool Wellcome Research Programme

Kondwani Jambo

Liverpool School of Tropical Medicine https://orcid.org/0000-0002-3195-2210

Article

Keywords: SARS-CoV-2, Upper Respiratory Tract, Lower Respiratory Tract, Antibodies, T cells

Posted Date: September 29th, 2026

DOI: https://doi.org/10.21203/rs.3.rs-10997315/v1

License: This work is licensed under a Creative Commons Attribution 4.0 International License.
Read Full License

Additional Declarations: There is **NO** Competing Interest.

Divergent systemic and airway mucosal adaptive immunity to SARS-CoV-2 in African adults

Author list

Gloria Kapira[1,2], Joseph A. Phiri[1], Robert K. Nyirenda[1], Memory N. Mvula[1], Edwin Lisimba[1], Austine D. Kumwenda[1], Dorothy Kazembe[1], Alice Kusakala[1], Anstead Kankwatira[1], Rose Malamba[1], Lucy Cooper[3], Mariana O. Diniz[3], Elena Mitsi[4], Mala Maini[3], Daniela M. Ferreira[4], Rhona M. Mijumbi[1,2], Henry C. Mwandumba[1,2,5], Kondwani C. Jambo[1,2,5]

Affiliations

[1]Malawi Liverpool Wellcome Research Programme, Blantyre, Malawi.

[2]Department of Clinical Sciences, Liverpool School of Tropical Medicine, L3 5QA, Liverpool, UK.

[3]University College London, UK

[4]Oxford Vaccine Group, Department of Paediatrics, NIHR Oxford Biomedical Research Centre, University of Oxford, OX3 9DU, UK

[5]Kamuzu University of Health Sciences, Blantyre, Malawi.

*Correspondence should be addressed to: G.K (gkapira@mlw.mw) and K.C.J (kjambo@mlw.mw)

Keywords: SARS-CoV-2, Upper Respiratory Tract, Lower Respiratory Tract, Antibodies, T cells

Abstract

Systemic antibody responses are more strongly associated with protection against severe COVID-19 in the lung than with protection against SARS-CoV-2 infection in the upper airway. To define the immunological basis of this divergence, we performed contemporaneous sampling of blood, nasal lining fluid (NLF), and bronchoalveolar lavage (BAL) fluid in HIV-uninfected adults and antiretroviral therapy (ART)-treated people with HIV (PWH). Serum spike-specific IgG antibodies correlated more strongly with BAL than with NLF across multiple variants of concern and were not confounded by HIV status. In contrast, IgA drove ACE2–spike inhibition activity in NLF, and this was not predicted by systemic or LRT antibodies. SARS-CoV-2–specific $CD4^+$ and $CD8^+$ T cells were enriched in BAL, exhibited tissue-resident phenotypes, and did not correlate with circulating T cells, even in ART-treated PWH. Together, these findings could provide an immunological basis for why systemic antibody responses reliably correlate with protection against lung disease but poorly predict nasal immunity.

Word count: 154 words

Introduction

SARS-CoV-2 continues to circulate globally despite widespread vaccination and prior infection [1]. Since the emergence of the Omicron variant, a key clinical shift has been observed: while lower respiratory tract (LRT) disease has declined substantially, upper respiratory tract (URT) infections remain common and continue to drive transmission [2, 3, 4, 5]. In Malawi, earlier waves dominated by the Beta and Delta variants of concern were associated with high rates of severe COVID-19 and mortality [6]. However, following the emergence of Omicron in December 2021, severe outcomes declined sharply, despite seroprevalence data indicating ongoing widespread exposure [3]. Consistent with this, a meta-analysis demonstrated significantly reduced protection against reinfection with Omicron BA.1, while protection against severe disease remained largely preserved [7]. Together, these observations suggest that the immune mechanisms preventing severe disease may differ from those required to block URT infection and onward transmission.

Systemic anti-Spike binding and neutralising antibodies are well-established correlates of protection (CoPs) against symptomatic COVID-19 and reliably predict protection against symptomatic disease [8, 9]. However, their predictive value for preventing URT infection or transmission is limited [10]. Parenteral COVID-19 vaccines induce robust systemic immunity but elicit relatively weak mucosal antibody responses in the respiratory tract [11, 12, 13, 14], and parenteral booster doses generate strong serum IgG but minimal mucosal IgA in saliva and nasal secretions in the absence of infection [15]. In contrast, intranasal vaccines induce potent local immunity and show promise for sterilising protection [11, 16, 17, 18], with clinical evidence demonstrating that intranasal administration of an adenovirus-vectored SARS-CoV-2 vaccine markedly increases spike-specific secretory IgA in the nasal mucosa [18]. These findings highlight a functional immunological divergence between compartments. However, the mechanisms underpinning this compartmentalisation, and its implications for defining CoPs against URT infection, remain incompletely understood. This suggests that additional immune parameters, including T cell responses and local mucosal humoral immunity, may be required to comprehensively assess protective immunity against SARS-CoV-2.

The impact of HIV infection on COVID-19 susceptibility and immune responses also remains incompletely defined [19]. Untreated HIV infection has been associated with prolonged SARS-CoV-2 shedding, accelerated viral evolution, and evidence of immune-driven selection [20, 21, 22]. In addition, impaired systemic SARS-CoV-2-specific T cell responses have been described in untreated HIV infection, characterised by reduced magnitude and diminished cross-recognition of variant epitopes compared with HIV-negative or treated aviraemic individuals [23]. Advanced HIV infection and low $CD4^+$ T cell counts have also been linked to suboptimal humoral responses to SARS-CoV-2 [24]. Although mucosal antibody responses are increasingly recognised as critical for limiting SARS-CoV-2 infection and transmission in the general population, direct assessment of respiratory tract mucosal immunity in people with HIV remains scarce. To date, only a single study has evaluated saliva antibodies in ART-treated people with HIV (PWH), reporting comparable neutralising activity to HIV-uninfected adults following BNT162b2 mRNA vaccination [25]. Thus, the absence of detailed studies interrogating respiratory mucosal immunity against SARS-CoV-2 in PWH represents a significant knowledge gap.

To address these gaps, we performed paired sampling of blood, nasal lining fluid (NLF), and bronchoalveolar lavage (BAL) in adults with and without HIV in Malawi. Using electrochemiluminescence immunoassays and multiparameter flow cytometry, we quantified SARS-CoV-2-specific antibody and T cell responses across systemic, upper, and lower respiratory compartments. This approach enabled us to define the compartment-specific architecture of antiviral immunity and to assess the impact of vaccination and treated HIV infection. Our findings provide insight into the limitations of systemic immune correlates for predicting URT protection and aim to inform future vaccine strategies and the development of more comprehensive CoP frameworks that incorporate mucosal as well as systemic immunity.

Results

Cohort characteristics and sampling

We recruited 91 adults in Blantyre, Malawi, comprising 45 HIV-uninfected adults and 46 asymptomatic people with HIV (PWH) on ART for more than one year. Nasal lining fluid (NLF), bronchoalveolar lavage (BAL) fluid, and peripheral blood were collected from all participants. Baseline characteristics, including median age and sex distribution, were different between the study groups (Table 1), with the PWH group being older (median 29 vs 40, p<0.001) and predominantly female (49% vs 74%, p=0.018). The median peripheral $CD4^+$ T cell count was 580 cells/µl (IQR 450–697) in ART-treated PWH. Detectable plasma viral load was observed in 15% (7/46) of ART-treated PWH.

Thirty-three per cent (15/45) of the HIV-uninfected adults were COVID-19 vaccinated, compared to 54% (25/46) of the ART-treated PWH. The time since last COVID-19 vaccination was similar between the two study groups (32 months vs 33 months, p=0.944). Thirty-three per cent (5/15) of the vaccinated HIV-uninfected adults received at least 2 doses, compared to 64% (16/25) in the ART-treated PWH group.

Systemic Spike IgG responses exhibit a stronger association with the lower than the upper respiratory tract

SARS-CoV-2 infection induces both systemic and mucosal antibodies; however, the extent to which immune responses are coordinated across respiratory compartments remains unclear. To address this, we quantified SARS-CoV-2–specific IgG and IgA antibodies in paired serum, NLF, and BAL samples from HIV-uninfected adults. We also examined the relationship between antibody responses across and within compartments.

All participants showed serological evidence of prior SARS-CoV-2 exposure, as indicated by detectable Nucleocapsid-specific antibodies, consistent with high community transmission in Malawi during successive epidemic waves [3, 6]. Wildtype (WT) Spike-, RBD- and Nucleocapsid-specific IgG titres exceeded IgA titres in serum, whereas WT Spike- and Nucleocapsid-specific

IgA predominated in NLF and Nucleocapsid-specific IgA in BAL, consistent with compartment-specific isotype skewing (Fig. 1a). IgG and IgA responses across compartments showed broadly similar binding breadth against SARS-CoV-2 WT and variants of concern (VOCs) (Fig. 1b). However, Delta Spike-specific IgA titres exceeded WT Spike-specific IgA titres across all compartments (Fig. 1b), consistent with its widespread circulation in Malawi prior to the emergence of Omicron [3, 6]. In contrast, Omicron Spike-specific IgG and IgA responses were broadly lower than WT Spike-specific responses across the compartments (Fig. 1b), in keeping with its reported immune-evasive properties [26].

We then examined the relationship between antibody responses across and within compartments. Serum IgG levels correlated strongly with BAL IgG across WT strain and all VOCs, whereas correlations between serum and NLF IgG were weak and only limited to Beta (Fig. 1c). Between BAL and NLF, IgA responses correlated for Beta and Gamma, but not for WT, Alpha, Delta and Omicron (Fig. 1c). Within serum, IgG and IgA responses showed no correlation across all variants, similarly no IgG–IgA correlations were observed within BAL for WT or any VOCs (Fig. 1c). In NLF, IgG and IgA correlations were restricted to WT and Alpha (Fig. 1c).

Furthermore, we measured inhibition of Spike–ACE2 binding to assess functional antibody activity. Serum demonstrated consistently higher neutralising activity than NLF across WT strain and all VOCs, with the lowest inhibition observed for Omicron in both compartments (Fig. 1d). Correlation analyses suggested that neutralisation in NLF was primarily IgA-mediated, whereas serum neutralisation was predominantly driven by IgG (Fig. 1e), consistent with prior observations [27]. IgG contributed minimally to ACE2 inhibition in NLF, particularly against Delta and Omicron.

Together, these findings indicate that systemic antibody responses are more closely aligned with the lower than the upper respiratory tract. The weak coupling between serum and NLF

responses, particularly for IgG and Omicron, underscores the compartmentalised nature of mucosal upper airway immunity and its limited reflection in systemic measurements.

Airway mucosal SARS-CoV-2–specific antibody responses are preserved in ART-treated PWH

ART-treated PWH generate SARS-CoV-2–specific antibody responses in blood that are broadly comparable to those of HIV-uninfected individuals [23]. However, whether mucosal SARS-CoV-2–specific antibody responses are similarly preserved across respiratory compartments remains unclear, particularly given evidence of persistent immune dysregulation at barrier sites despite systemic viral suppression [28]. To address this, we compared Spike-, RBD- and Nucleocapsid-specific IgA and IgG responses in serum, BAL, and NLF by HIV status. WT Spike-, RBD-, and Nucleocapsid-specific IgA and IgG responses in serum, BAL, and NLF did not differ significantly between ART-treated PWH and HIV-uninfected participants (Fig. 2a-b). Similarly, the ACE2 inhibition against WT and multiple VOCs was comparable between the two groups in both serum and NLF (Fig. 2c). These findings indicate that mucosal humoral immunity is largely preserved in ART-treated PWH.

Serum and mucosal correlates of potential anti-SARS-CoV-2 neutralising immunity vary across the upper and lower airway compartments

Antibody-mediated neutralisation is a key mechanism of protection against SARS-CoV-2 infection [29, 30]. Given the observed compartmentalisation of humoral responses, we next sought to identify immunological markers most strongly associated with functional antibody activity across the respiratory tract and systemic circulation. Because direct neutralisation assays in BAL were not feasible due to dilutional constraints, BAL anti-Spike IgG was used as a surrogate marker of neutralisation potential in the lower respiratory tract. In the URT and serum, ACE2 inhibition served as the readout of neutralisation capacity. For each participant, we calculated the breadth of anti-Spike SARS-CoV-2–specific binding IgG, binding IgA, and ACE2 inhibition as the median response across Wildtype and four SARS-CoV-2 variants of concern and included these measures in multivariable linear regression models.

We applied multivariable linear regression models incorporating demographic and immunological variables to identify predictors of NLF and serum ACE2 inhibition breadth and BAL anti-Spike IgG binding breadth (Table 2). NLF ACE2 inhibition breadth was most strongly associated with local anti-Spike IgA binding breadth ($\beta = 0.62$, $p < 0.001$), with a smaller contribution from NLF IgG binding breadth ($\beta = 0.26$, $p = 0.008$). In contrast, serum ACE2 inhibition breadth was strongly associated with serum IgG binding breadth ($\beta = 0.68$, $p < 0.001$), whereas the contribution of serum IgA binding breadth was not statistically significant ($\beta = 0.12$, $p = 0.148$). In the LRT, BAL anti-Spike IgG binding breadth was associated with serum IgG binding breadth ($\beta = 0.50$, $p < 0.001$) and BAL IgA binding breadth ($\beta = 0.52$, $p < 0.001$). Demographic variables, including age, sex, HIV status, and vaccination status, were not significant predictors of these outcomes. These findings identify anatomically distinct correlates of potential anti-SARS-CoV-2 neutralising immunity, with systemic IgG responses aligning more closely with the lower respiratory tract, whereas local IgA predominates as a correlate of neutralisation capacity in the upper airway.

SARS-CoV-2-specific T cell responses are enriched in the lung, uncoupled from antibody levels and largely preserved under suppressive ART

Given the close alignment between serum and BAL antibody responses, we next assessed whether SARS-CoV-2–specific T cell responses were similarly coordinated across compartments. Using intracellular cytokine staining following stimulation with overlapping peptides, we quantified WT Spike- and WT Nucleocapsid-specific $CD4^+$ and $CD8^+$ T cells in BAL and blood samples. Representative flow cytometry plots illustrate SARS-CoV-2–specific $CD4^+$ and $CD8^+$ T cell responses detected in BAL and blood (Fig. 3a). Spike- and Nucleocapsid-specific $CD4^+$ T cell frequencies were significantly higher in BAL than in blood (Fig. 3b). Similarly, Nucleocapsid-specific $CD8^+$ T cell frequencies were significantly higher in BAL than in blood (Fig. 3c), whereas only a non-significant trend was observed for Spike-specific $CD8^+$ T cells. Spike- and Nucleocapsid-specific $CD4^+$ T cell and $CD8^+$ T cell frequencies were positively correlated within each compartment. Moreover, no association was observed between antibody levels and T cell frequencies within compartments (Fig. 3d).

Comparisons between ART-treated PWH and HIV-uninfected individuals revealed broadly similar Spike- and Nucleocapsid-specific $CD4^+$ and $CD8^+$ T cell frequencies in both BAL and blood (Fig. 4a–b). However, Nucleocapsid-specific $CD8^+$ T cells in BAL showed a trend towards lower frequencies in ART-treated PWH compared to HIV-uninfected individuals. No significant correlations were observed between BAL and blood Spike- and Nucleocapsid-specific $CD4^+$ or $CD8^+$ T cell frequencies (Fig. 4c–d). Together, these data indicate that SARS-CoV-2–specific T cell responses are compartmentalised, enriched in the lung, largely preserved under suppressive ART, and not reliably reflected in peripheral blood.

SARS-CoV-2–specific T cells exhibit compartment-specific phenotypic divergence

To further characterise compartmental divergence, we performed phenotypic profiling of WT Spike- and WT Nucleocapsid-specific $CD4^+$ and $CD8^+$ T cells from BAL and blood, pooling data across vaccination and HIV status. Spike- and Nucleocapsid-specific $CD4^+$ T cells in BAL exhibited phenotypes enriched for CD69 expression with limited CD103 co-expression and a TNFα-dominant cytokine profile (Fig. 5a). In contrast, Spike- and Nucleocapsid-specific $CD4^+$ T cells in blood were predominantly $CD69^-CD103^-$ with IFNγ and/or TNFα production, reflecting a systemic effector phenotype (Fig. 5a).

On the other hand, Spike- and Nucleocapsid-specific $CD8^+$ T cells showed even clearer compartmental divergence (Fig. 5b). In BAL, Spike- and Nucleocapsid-specific $CD8^+$ T cells were dominated by $CD103^+CD69^+$ phenotypes with IFNγ and/or TNFα production, consistent with tissue-resident memory (TRM)–associated markers. In contrast, blood Spike- and Nucleocapsid-specific $CD8^+$ T cells were predominantly $CD69^-CD103^-$ and produced IFNγ or TNFα.

Together, these findings demonstrate that SARS-CoV-2–specific T cells exhibit pronounced compartment-specific phenotypic differentiation, with BAL populations displaying features consistent with tissue residency and functional potential that is not recapitulated in peripheral blood.

Discussion

Despite widespread COVID-19 vaccination and natural infection, SARS-CoV-2 continues to circulate globally, driven by persistent URT infection and transmission even in highly vaccinated populations[1]. Prior infection or vaccination confers substantially stronger protection against LRT disease than against URT infection[7]. This clinical divergence is mirrored immunologically; serum anti-Spike IgG neutralising antibodies are established correlates of protection against severe COVID-19 but are less predictive of URT infection or transmission [8, 9, 10]. To investigate the immunological basis for this compartment-specific dissociation, we performed contemporaneous sampling of serum, BAL, and NLF, enabling direct comparison of immune responses across systemic, upper, and lower airway compartments.

Our data demonstrate that systemic antibody responses, particularly serum anti-Spike IgG, align more closely with immunity in the lower respiratory tract (LRT) than in the upper respiratory tract (URT). BAL anti-Spike IgG titres correlated strongly with serum neutralisation, consistent with prior observations in other settings [31], and suggesting shared induction pathways or IgG transudation into the alveolar space [32]. In contrast, functional antibody activity in NLF was primarily driven by local IgA and was poorly predicted by systemic or LRT antibody responses. This compartmentalisation likely reflects fundamental differences in immune induction and maintenance across the respiratory tract. Whereas IgG in the lower airway may be sustained through systemic immune memory and transudation, immunity in the upper airway appears to rely predominantly on locally induced IgA, which may be more transient and exposure-dependent [33, 34]. These kinetic differences may contribute to the dissociation between protection from severe disease and susceptibility to URT infection.

The limited association between systemic or LRT antibodies and URT neutralising activity may help explain the reduced performance of serum neutralisation assays as correlates of protection for URT infection [35]. Although serum anti-Spike IgG and BAL IgA showed modest associations with NLF antibody levels, they did not independently predict URT neutralisation.

This is particularly relevant in the context of intramuscular SARS-CoV-2 vaccines, which, while highly effective at preventing severe disease, often fail to elicit robust or durable mucosal antibody responses in the respiratory tract [11, 36]. In contrast, vaccination strategies combining intramuscular priming with intranasal boosting elicit strong mucosal IgA and neutralising responses [37, 38, 39]. Collectively, these findings underscore the importance of incorporating mucosal immune endpoints into vaccine evaluation and support the development of mucosal vaccine platforms to achieve sterilising immunity and reduce transmission.

Beyond humoral immunity, we identified marked compartmentalisation of SARS-CoV-2–specific T cell responses. Antigen-specific $CD4^+$ and $CD8^+$ T cells were significantly enriched in BAL compared with blood, consistent with observations in other respiratory infections, including *Mycobacterium tuberculosis* and influenza virus [40, 41]. Moreover, BAL SARS-CoV-2–specific T cells exhibited phenotypic profiles distinct from those in blood. In particular, $CD8^+$ T cells in BAL were biased toward a tissue-resident memory (TRM) phenotype, defined by CD69 and CD103 expression [42, 43]. TRM cells mediate rapid, localised immune responses and are thought not to recirculate [43], consistent with the absence of a correlation between BAL and blood T cell frequencies. The enrichment of TRM-associated phenotypes in BAL, together with the lack of correlation with blood responses, supports the concept that lung-resident T cell immunity is compartmentalised and not adequately captured by peripheral sampling.

Our cohort included a substantial proportion of PWH receiving suppressive ART, most of whom had undetectable viral load and preserved $CD4^+$ T cell counts. In this context, SARS-CoV-2–specific systemic and mucosal antibody responses, as well as T cell responses, were broadly comparable between ART-treated PWH and HIV-uninfected individuals. These findings are consistent with data from South Africa showing that impaired SARS-CoV-2–specific $CD4^+$ T cell responses were confined to viraemic individuals and were not observed in those on suppressive ART [23]. While uncontrolled HIV infection has been associated with prolonged SARS-CoV-2 shedding [20, 44], our data indicate that responses were broadly comparable among ART-treated PWH and HIV-uninfected participants in both systemic and airway mucosal

immune responses, aligning with growing evidence that well-controlled HIV infection does not confer increased risk of severe COVID-19 or prolonged viral shedding [19].

Several limitations should be acknowledged. First, the cross-sectional design precludes definitive inference regarding the timing, durability, or variant-specific dynamics of immune responses, and waning or boosting over time may differentially affect responses across compartments. Second, quantification of mucosal immune responses is subject to technical variability related to sampling and dilution, particularly in BAL. Owing to low antibody concentrations resulting from lavage dilution, direct neutralisation or pseudo-neutralisation assays could not be performed on BAL samples. In addition, although ACE2 inhibition represents a surrogate rather than authentic virus neutralisation, it provides a scalable and informative functional readout that has been widely applied in prior studies to assess neutralising activity, including in mucosal samples [45]. Finally, the absence of clinical endpoints, such as infection or disease outcomes, limits direct inference regarding protection. Longitudinal studies linking compartment-specific immunity to prospective infection risk will be required to validate these associations. Nonetheless, the immune parameters assessed here, including binding antibodies, surrogate neutralisation measures, and functional T cell responses, are closely linked to protective immunity.

In summary, this study provides an immunological framework that may explain why systemic antibody responses reliably correlate with protection against LRT disease but poorly predict URT immunity to SARS-CoV-2. While serum anti- SARS-CoV-2 IgG reflects protective immunity in the lung as previously reported [31], it fails to capture neutralising capacity in the upper airway, where local IgA predominates as shown in this study. These findings highlight the need to incorporate mucosal immune measures into future correlates-of-protection studies and suggest that alternative vaccine strategies, including mucosal delivery, may be required to achieve durable protection against SARS-CoV-2 infection and transmission.

Methods

Study design and participants

This cross-sectional study was conducted at the Malawi-Liverpool-Wellcome Research Programme (MLW) in Blantyre, Malawi, to investigate respiratory mucosal immune responses to SARS-CoV-2. We recruited healthy adults aged 18 to 65 years with a history of prior SARS-CoV-2 infection from Queen Elizabeth Central Hospital (QECH), Blantyre, Malawi. Participants included HIV-uninfected adults and clinically asymptomatic PWH who were receiving ART for more than 1 year and attending routine follow-up visits at HIV care clinics. COVID-19 vaccination history, including vaccine type, number of doses, vaccination dates, and booster status, was verified using the health passport records. HIV status was confirmed using the national rapid diagnostic testing algorithm (two independent rapid tests), with polymerase chain reaction (PCR) used for confirmation in PWH on ART. ART duration and regimen were verified from the health passport book. Participants were excluded if they had active SARS-CoV-2 infection, poor clinical status, or contraindications to bronchoscopy, were pregnant, had recent tuberculosis treatment, chronic respiratory or systemic comorbidities, hypoxaemia (SaO_2 <90%), significant anaemia or bleeding disorders, known allergies to study medications used during bronchoscopy (including lignocaine), recent smoking exposure, or if informed consent was not provided.

Sample collection

We obtained peripheral blood samples by venepuncture. At the screening visit, whole blood was collected into EDTA tubes for full blood count, CD4 count, and HIV viral load measurement. At the enrolment visit, conducted 2 days after screening, whole blood was collected into sodium heparin and serum separator tubes. Peripheral blood mononuclear cells (PBMCs) were isolated from whole blood within 2 h of collection by density-gradient centrifugation using Lymphoprep (Fisher Scientific, UK). Cells were washed twice in phosphate-buffered saline (PBS; Thermo Fisher Scientific, UK) and counted by trypan blue exclusion (Sigma-Aldrich). PBMCs were used immediately for intracellular cytokine assays. Plasma was separated by centrifugation at 1,500 × g for 10 min. Serum was aliquoted and

stored at −80 °C for subsequent antibody analysis using a multiplex Meso Scale Discovery (MSD) immunoassay.

Nasal lining fluid (NLF) was collected using a synthetic absorptive matrix (Hunts Development Ltd, UK), eluted in 200 µL PBS (Fisher Scientific), and centrifuged at 1,500 × g for 10 min. The eluate was stored at −80 °C until antibody analysis using a multiplex MSD immunoassay. A full list of reagents is provided in Supplementary Table 1.

Bronchoalveolar lavage (BAL) was collected using a flexible fibreoptic bronchoscope, instilling 200 mL of sterile saline (0.9% NaCl) into the right middle lobe, with gentle suction applied after each instillation. BAL samples were processed within 1 h of collection. BAL fluid was filtered through a sterile 100 µm cell strainer and centrifuged at 500 × g for 10 min at 4 °C. The cell pellet was resuspended in RPMI 1640 medium (Fisher Scientific) supplemented with 10% fetal bovine serum (Sigma-Aldrich). Cell viability was assessed by trypan blue exclusion (Sigma-Aldrich). BAL cells were used immediately for intracellular cytokine assays. Cell-free BAL supernatant was aliquoted and stored at −80 °C for subsequent antibody analyses using a multiplex MSD immunoassay.

SARS-CoV-2 serology

A Meso Scale Discovery (MSD) immunoassay was used to measure SARS-CoV-2 IgG and IgA antibody titres against three viral proteins: wildtype (WT) Nucleocapsid, WT receptor-binding domain (RBD) and WT Spike. The assay was performed using a 10-spot MULTI-SPOT 96-WELL plate that was pre-coated with different SARS-CoV-2 antigens, including: WT Nucleocapsid, WT RBD and WT Spike and Spike VOCs antigens for Alpha, Beta, Gamma, Delta, and Omicron (B.1.1.529), following the manufacturer's instructions. In summary, the plates were blocked with MSD Blocker A, and reference standards, controls and samples (serum IgA 1:5,000, serum IgG 1:5,000; NLF IgA 1:500, NLF IgG 1:10; BAL supernatant IgA 1:100, BAL supernatant IgG 1:10) diluted in diluent buffer were then added. After incubation, a detection antibody was added (MSD SULFO-TAG™ Anti-Human IgG or IgA Antibody), followed by the addition of MSD GOLD™

Read Buffer B. The plates were then read using a MESO® QuickPlex SQ 120 MM Reader. As per the manufacturer's instructions for the MSD kit, only the WT Spike, WT RBD and WT Nucleocapsid have measurements in both World Health Organisation Binding Antibody Units (WHO BAU/ml) and MSD Arbitrary Units (MSD AU/ml). However, antibody measurements for the Spike variants of concern are reported only in MSD AU/mL and are not yet calibrated to WHO BAU/ml units. Furthermore, BAL samples were adjusted with a dilution factor of 100, based on our unpublished urea assay results from prior work, while the NLF was adjusted to a dilution factor of 20 based on the elution volume used.

ACE2 inhibition (surrogate neutralisation) assay

A quantitative COVID-19 Angiotensin-converting enzyme 2 (ACE2) Neutralisation MSD 10-spot MULTI-SPOT® 96-well plate was used to measure neutralisation capacity, following the manufacturer's instructions. The plate was pre-coated with SARS-CoV-2 viral antigens and then blocked with MSD Blocker A for 30 minutes. Prepared reference standards and diluted samples (serum [1:20] and NLF [1:20]) in diluent buffer were added, then incubated for 2 hours. After that, the ACE2 detection antibody (SULFO-TAG Human ACE2 Protein) was added and incubated for 60 minutes. Finally, MSD GOLD™ Read Buffer B was added, and plates were read using a MESO® QuickPlex SQ 120 MM Reader.

T cell stimulation and intracellular cytokine staining

PBMCs and BAL cells were stimulated with PepTivator SARS-CoV-2 Prot_N, a pool of lyophilised peptides covering the complete nucleocapsid protein sequence (GenBank MN908947.3, Protein QHD43423.2, Miltenyi Biotec, UK), or PepTivator SARS-CoV-2 Prot_S complete, covering the full spike glycoprotein sequence (aa 5–1273; GenBank MN908947.3, Protein QHD43416.1, Miltenyi Biotec, UK), in the presence of co-stimulatory antibodies (anti-CD28 and anti-CD49d; BD Biosciences), Brefeldin A (BD GolgiPlug™, BD Biosciences) for 18 h at 37 °C. Cells stimulated with Cell Activation Cocktail (phorbol 12-myristate 13-acetate [PMA] and ionomycin, without Brefeldin A; BioLegend) served as positive controls, whereas unstimulated cells served as negative controls.

Following 18 h stimulation, cells were harvested and stained with LIVE/DEAD fixable aqua amine-reactive dye (Thermo Fisher Scientific), followed by surface fluorochrome-labelled monoclonal antibodies: APC anti-human CD3, APC-Cy7 anti-human CD4, Alexa Fluor 700 anti-human CD8, Brilliant Violet 605 anti-human CD69, and PE-Cy7 anti-human CD103 (all BioLegend; antibody details in Supplementary Table 1). Cells were then fixed and permeabilised using Fixation/Permeabilisation solution (Thermo Fisher Scientific) for 40 min, washed in permeabilisation buffer (Thermo Fisher Scientific), and stained intracellularly with PE anti-human IFN-γ and FITC anti-human TNF-α (BioLegend; antibody details in Supplementary Table 1).

Flow cytometry acquisition and analysis

PBMCs and BAL samples were acquired on a BD LSRFortessa™ flow cytometer using FACSDiva v.9.2 (BD Biosciences), and data were analysed using FlowJo v10.10.0 (BD Biosciences). Compensation was performed using single-stained compensation beads (BD CompBeads), and gates were set using unstimulated controls. Doublets and dead cells were excluded before analysis. T cells were identified as $CD3^+$ lymphocytes and further subdivided into $CD4^+$ and $CD8^+$ populations. Cytokine-producing cells were defined as IFN-γ^+ and/or TNF-α^+ after background subtraction of unstimulated controls. The gating strategy is shown in Supplementary Fig. 1.

Ethics statement

The study was conducted in accordance with the Declaration of Helsinki and adhered to good clinical practice as well as local and international institutional guidelines. Ethical approval was obtained from the National Health Sciences Research Committee (protocol no. AD23/03/4018, Malawi) and the Liverpool School of Tropical Medicine Research Ethics Committee (protocol no. 23-026, UK). Written informed consent was obtained from all participants before enrolment. Participants received compensation in accordance with approved ethical guidelines.

Statistical analysis

All statistical analyses were performed using R (version 4.5.2). Paired antibody responses were compared using two-sided Wilcoxon signed-rank tests, whereas comparisons between independent groups for T cell responses were performed using two-sided non-parametric Wilcoxon rank-sum tests. Correlations were assessed using Spearman's rank correlation coefficient and interpreted with emphasis on consistent patterns observed across compartments, variants and viral antigens. P values from comparisons and correlation analyses of antibody responses were adjusted for multiple testing using the Benjamini–Hochberg false discovery rate (FDR) method. Multivariable linear regression models were used to identify predictors of antibody responses, adjusting for age, sex, HIV status and vaccination status. Statistical significance was defined as a two-sided $P < 0.05$. Details of statistical tests and sample sizes for each analysis are provided in the corresponding figure legends.

Data availability

The source data generated in this study have been deposited in a GitHub repository and are accessible through https://github.com/glorialuhanga/Divergent-systemic-and-airway-mucosal-adaptive-immunity-to-SARS-CoV-2-in-African-adults.

Code availability

The manuscript code and R scripts used to analyse the datasets are available in the GitHub repository https://github.com/glorialuhanga/Divergent-systemic-and-airway-mucosal-adaptive-immunity-to-SARS-CoV-2-in-African-adults.

Acknowledgements

This work was supported by a Wellcome grant (226131/Z/22/Z) to K.C.J, H.C.M, R.M.M., D.M.F, M.M, E.M and M.O.D. We are grateful to all the study participants.

Author contributions

Conceptualisation and supervision: K.C.J., M.M., D.M.F., and H.C.M.; Data curation: G.K., K.C.J.; Data analysis: G.K., K.C.J.; Interpretation: G.K., K.C.J.; Funding acquisition: K.C.J., H.C.M., R.M.M., D.M.F., M.M., E.M. and M.O.D.; Investigation: D.K., A.K.1; Methodology: G.K., J.A.P., R.K.N., M.N.M., E.L. and A.D.K.; Project administration: D.K.; Community engagement: G.K., R.K.N., A.K.1, D.K., R.M., R.M.M., K.C.J.; Sample collection: A.K.2, R.M. and A.K.1; Validation: G.K., K.C.J.; Writing–original draft: G.K., K.C.J.; Writing–review and editing: G.K., J.A.P., R.K.N., M.N.M., E.L., A.D.K., R.M., L.C., M.O.D., E.M., M.M., D.M.F., R.M.M., and K.C.J. All authors reviewed and approved the final version of the manuscript.

Competing interests

The authors declare no competing interests.

References

1. WHO. COVID-19 - Global Situation. 2025 28 May 2025 [cited]Available from: https://www.who.int/emergencies/disease-outbreak-news/item/2025-DON572#:~:text=Since%20mid%2DFebruary%202025%2C%20according%20to,been%20observed%20since%20July%202024.).

2. Wickenhagen, A. *et al.* Evolution of Omicron lineage towards increased fitness in the upper respiratory tract in the absence of severe lung pathology. *Nat Commun* **16**, 594 (2025).

3. Mseka, U.L. *et al.* Omicron B.1.1.529 variant infections associated with severe disease are uncommon in a COVID-19 under-vaccinated, high SARS-CoV-2 seroprevalence population in Malawi. *eClinicalMedicine* **56** (2023).

4. Madhi, S.A., Ihekweazu, C., Rees, H. & Pollard, A.J. Decoupling of omicron variant infections and severe COVID-19. *The Lancet* **399**, 1047-1048 (2022).

5. Madhi, S.A. *et al.* Population Immunity and Covid-19 Severity with Omicron Variant in South Africa. *N Engl J Med* **386**, 1314-1326 (2022).

6. JHU. COVID-19 Case Tracker 2020 [cited]Available from: https://coronavirus.jhu.edu/map.html.

7. Stein, C. *et al.* Past SARS-CoV-2 infection protection against re-infection: a systematic review and meta-analysis. *The Lancet* **401**, 833-842 (2023).

8. Khoury, D.S. *et al.* Neutralizing antibody levels are highly predictive of immune protection from symptomatic SARS-CoV-2 infection. *Nat Med* **27**, 1205-1211 (2021).

9. Goldblatt, D., Alter, G., Crotty, S. & Plotkin, S.A. Correlates of protection against SARS-CoV-2 infection and COVID-19 disease. *Immunological Reviews* **310**, 6-26 (2022).

10. Sun, K. *et al.* SARS-CoV-2 correlates of protection from infection against variants of concern. *Nat Med* **30**, 2805-2812 (2024).

11. Pilapitiya, D., Wheatley, A.K. & Tan, H.-X. Mucosal vaccines for SARS-CoV-2: triumph of hope over experience. *eBioMedicine* **92** (2023).

12. Azzi, L. *et al.* Mucosal immune response in BNT162b2 COVID-19 vaccine recipients. *EBioMedicine* **75**, 103788 (2022).

13. Tang, J. *et al.* Respiratory mucosal immunity against SARS-CoV-2 after mRNA vaccination. *Science Immunology* **7**, eadd4853 (2022).

14. Fraser, R., Orta-Resendiz, A., Mazein, A. & Dockrell, D.H. Upper respiratory tract mucosal immunity for SARS-CoV-2 vaccines. *Trends in Molecular Medicine* **29**, 255-267 (2023).

15. Bhavsar, D. *et al.* Mucosal antibody responses to SARS-CoV-2 booster vaccination and breakthrough infection. *mBio* **14**, e02280-02223 (2023).

16. Mao, T. *et al.* Unadjuvanted intranasal spike vaccine elicits protective mucosal immunity against sarbecoviruses. *Science* **378**, eabo2523 (2022).

17. Hong, W. *et al.* Intranasal vaccine combining adenovirus and trimeric subunit protein provides superior immunity against SARS-CoV-2 Omicron variant. *Nature Biomedical Engineering* (2025).

18. Sun, B. *et al.* An intranasally administered adenovirus-vectored SARS-CoV-2 vaccine induces robust mucosal secretory IgA. *JCI Insight* **9** (2024).

19. Höft, M.A., Burgers, W.A. & Riou, C. The immune response to SARS-CoV-2 in people with HIV. *Cell Mol Immunol* **21**, 184-196 (2024).

20. Velasquez-Reyes, J.M. *et al.* Characterisation of a persistent SARS-CoV-2 infection lasting more than 750 days in a person living with HIV: a genomic analysis. *The Lancet Microbe* **6** (2025).

21. Cele, S. *et al.* SARS-CoV-2 prolonged infection during advanced HIV disease evolves extensive immune escape. *Cell Host Microbe* **30**, 154-162.e155 (2022).

22. Ko, S.H. *et al.* Rapid intra-host diversification and evolution of SARS-CoV-2 in advanced HIV infection. *Nat Commun* **15**, 7240 (2024).

23. Nkosi, T. *et al.* Unsuppressed HIV infection impairs T cell responses to SARS-CoV-2 infection and abrogates T cell cross-recognition. *eLife* **11**, e78374 (2022).

24. Ruta, S. *et al.* SARS-CoV-2 Humoral and Cellular Immune Responses in People Living with HIV. *Vaccines* **12**, 663 (2024).

25. Schmidt, K.G. *et al.* Characterization of Serum and Mucosal SARS-CoV-2-Antibodies in HIV-1-Infected Subjects after BNT162b2 mRNA Vaccination or SARS-CoV-2 Infection. *Viruses* **14**, 651 (2022).

26. Willett, B.J. *et al.* SARS-CoV-2 Omicron is an immune escape variant with an altered cell entry pathway. *Nature Microbiology* **7**, 1161-1179 (2022).

27. Puhach, O. *et al.* SARS-CoV-2 convalescence and hybrid immunity elicits mucosal immune responses. *eBioMedicine* **98** (2023).

28. Phiri, J.A. *et al.* Persistent pneumococcal colonisation in antiretroviral-treated HIV infection is associated with nasal inflammation. *Nat Commun* **17**, 565 (2025).

29. Feng, S. *et al.* Correlates of protection against symptomatic and asymptomatic SARS-CoV-2 infection. *Nature Medicine* **27**, 2032-2040 (2021).

30. Addetia, A. *et al.* Neutralizing Antibodies Correlate with Protection from SARS-CoV-2 in Humans during a Fishery Vessel Outbreak with a High Attack Rate. *Journal of Clinical Microbiology* **58**, 10.1128/jcm.02107-02120 (2020).

31. Padawer, D. *et al.* BNT162b2 vaccine induces potent SARS-CoV-2 neutralising immunoglobulins in lung mucosa. *ERJ Open Research* **11**, 00269-02025 (2025).

32. Kim, K.J. & Malik, A.B. Protein transport across the lung epithelial barrier. *Am J Physiol Lung Cell Mol Physiol* **284**, L247-259 (2003).

33. Marking, U. *et al.* Impact of systemic SARS-CoV-2 vaccination on mucosal IgA responses to subsequent breakthrough infection. *eBioMedicine* **120** (2025).

34. Escalera, A. *et al.* SARS-CoV-2 infection induces robust mucosal antibody responses in the upper respiratory tract. *iScience* **27**, 109210 (2024).

35. Chen, S. *et al.* Nasal mucosal secretory immunoglobulin A but not serum antibodies is resistant to Omicron evasion. *hLife* **2**, 488-491 (2024).

36. Winklmeier, S. *et al.* Intramuscular vaccination against SARS-CoV-2 transiently induces neutralizing IgG rather than IgA in the saliva. *Frontiers in Immunology* **Volume 15 - 2024** (2024).

37. Laghlali, G. *et al.* Enhanced mucosal SARS-CoV-2 immunity after heterologous intramuscular mRNA prime/intranasal protein boost vaccination with a combination adjuvant. *Molecular Therapy* **32**, 4448-4466 (2024).

38. Tang, J. *et al.* Intramuscular mRNA prime plus intranasal adenoviral vector booster elicit robust respiratory mucosal IgA responses against SARS-CoV-2. *The Journal of Immunology* **210**, 253.214-253.214 (2023).

39. Lin, Y. *et al.* Sequential intranasal booster triggers class switching from intramuscularly primed IgG to mucosal IgA against SARS-CoV-2. *J Clin Invest* **135** (2025).

40. Jambo, K.C. *et al.* Asymptomatic HIV-infected individuals on antiretroviral therapy exhibit impaired lung CD4(+) T-cell responses to mycobacteria. *Am J Respir Crit Care Med* **190**, 938-947 (2014).

41. Jambo, K.C. *et al.* Bronchoalveolar CD4+ T cell responses to respiratory antigens are impaired in HIV-infected adults. *Thorax* **66**, 375-382 (2011).

42. Zheng, M.Z.M. & Wakim, L.M. Tissue resident memory T cells in the respiratory tract. *Mucosal Immunol* **15**, 379-388 (2022).

43. Kumar, B.V. *et al.* Human Tissue-Resident Memory T Cells Are Defined by Core Transcriptional and Functional Signatures in Lymphoid and Mucosal Sites. *Cell Reports* **20**, 2921-2934 (2017).

44. Meiring, S. *et al.* Prolonged Shedding of Severe acute respiratory syndrome coronavirus 2 (SARS-CoV-2) at High Viral Loads Among Hospitalized

Immunocompromised Persons Living With Human Immunodeficiency Virus (HIV), South Africa. *Clinical Infectious Diseases* **75**, e144-e156 (2022).

45. Fröberg, J. *et al.* Primary Exposure to SARS-CoV-2 via Infection or Vaccination Determines Mucosal Antibody-Dependent ACE2 Binding Inhibition. *The Journal of Infectious Diseases* **229**, 137-146 (2023).

Tables

Table 1 | Participant demographics and clinical characteristics

Characteristic	HIV-uninfected N = 45[1]	PLHIV ART>1yr N = 46[1]	p-value[2]
Age (years)	29 (24, 37)	40 (35, 44)	<0.001
Sex			0.018
Female	22 (49%)	34 (74%)	
Male	23 (51%)	12 (26%)	
Vaccination status			0.071
Unvaccinated	30 (67%)	21 (46%)	
Vaccinated	15 (33%)	25 (54%)	
Number of doses			0.120
1	10 (67%)	9 (36%)	
2	5 (33%)	16 (64%)	
Primary vaccine type (Dose 1)			0.259
AstraZeneca	10 (67%)	15 (60%)	
Janssen (Johnson & Johnson)	4 (27%)	6 (24%)	
Moderna	0 (0%)	4 (16%)	
Pfizer-BioNTech	1 (7%)	0 (0%)	
Primary vaccine type (Dose 2)			0.589
AstraZeneca	4 (80%)	10 (63%)	
Janssen (Johnson & Johnson)	1 (20%)	2 (13%)	
Moderna	0 (0%)	4 (25%)	
Time since last COVID-19 vaccination (months)	32 (23, 37)	33 (23, 36)	0.944
Absolute CD4 cell count (cells/µL)	NA (NA, NA)	580 (450, 697)	
HIV viral load			
Not Detected	0 (NA%)	39 (85%)	
Detected	0 (NA%)	7 (15%)	

[1] Median (Q1, Q3); n (%)

[2] Wilcoxon rank sum test; Fisher's exact test; Pearson's Chi-squared test

Table 2 | Linear regression analysis of immunological markers and demographic factors

Predictor	NLF neutralization breadth β (95% CI)	p	Serum neutralization breadth β (95% CI)	p	BAL IgG binding breadth β (95% CI)	p
Participant characteristics						
Age	0.00 (-0.18, 0.18)	0.958	0.11 (-0.04, 0.26)	0.150	0.05 (-0.15, 0.25)	0.621
Sex (Male)	-0.09 (-0.42, 0.24)	0.586	-0.11 (-0.38, 0.16)	0.432	-0.21 (-0.58, 0.16)	0.252
HIV+ status	0.16 (-0.20, 0.51)	0.384	-0.20 (-0.50, 0.09)	0.170	-0.09 (-0.50, 0.31)	0.648
Vaccinated	0.01 (-0.34, 0.35)	0.964	0.02 (-0.26, 0.31)	0.867	-0.08 (-0.47, 0.31)	0.670
Systemic markers						
Serum IgG binding breadth	-0.14 (-0.36, 0.08)	0.208	**0.68 (0.50, 0.86)**	**<0.001**	**0.50 (0.28, 0.72)**	**<0.001**
Serum IgA binding breadth	0.05 (-0.14, 0.25)	0.584	0.12 (-0.04, 0.28)	0.148	-0.19 (-0.41, 0.03)	0.091
Lower airway markers						
BAL IgG binding breadth	-0.15 (-0.35, 0.06)	0.154	0.10 (-0.06, 0.27)	0.222	—	—
BAL IgA binding breadth	-0.07 (-0.26, 0.13)	0.497	-0.10 (-0.25, 0.06)	0.231	**0.52 (0.34, 0.70)**	**<0.001**
Upper airway markers						
NLF IgG binding breadth	**0.26 (0.07, 0.44)**	**0.008**	0.10 (-0.05, 0.26)	0.187	0.15 (-0.06, 0.36)	0.162
NLF IgA binding breadth	**0.62 (0.43, 0.81)**	**<0.001**	0.05 (-0.10, 0.21)	0.502	-0.15 (-0.36, 0.06)	0.167

Multivariable linear regression models fitted on n = 86 participants. β values are standardized coefficients.

Linear regression models were used to assess associations between immunological markers (breadth of anti-Spike SARS-CoV-2–specific binding IgG, anti-Spike SARS-CoV-2–specific binding IgA, and ACE2 inhibition) and demographic variables (age, sex, HIV and vaccination status). Breadth was defined as the median response across Wildtype and four SARS-CoV-2 variants of concern for each participant. Values represent regression coefficients (β) with 95% confidence intervals; p-values indicate statistical significance (*p < 0.05).

Figures and Figure Legends

Figure 1.

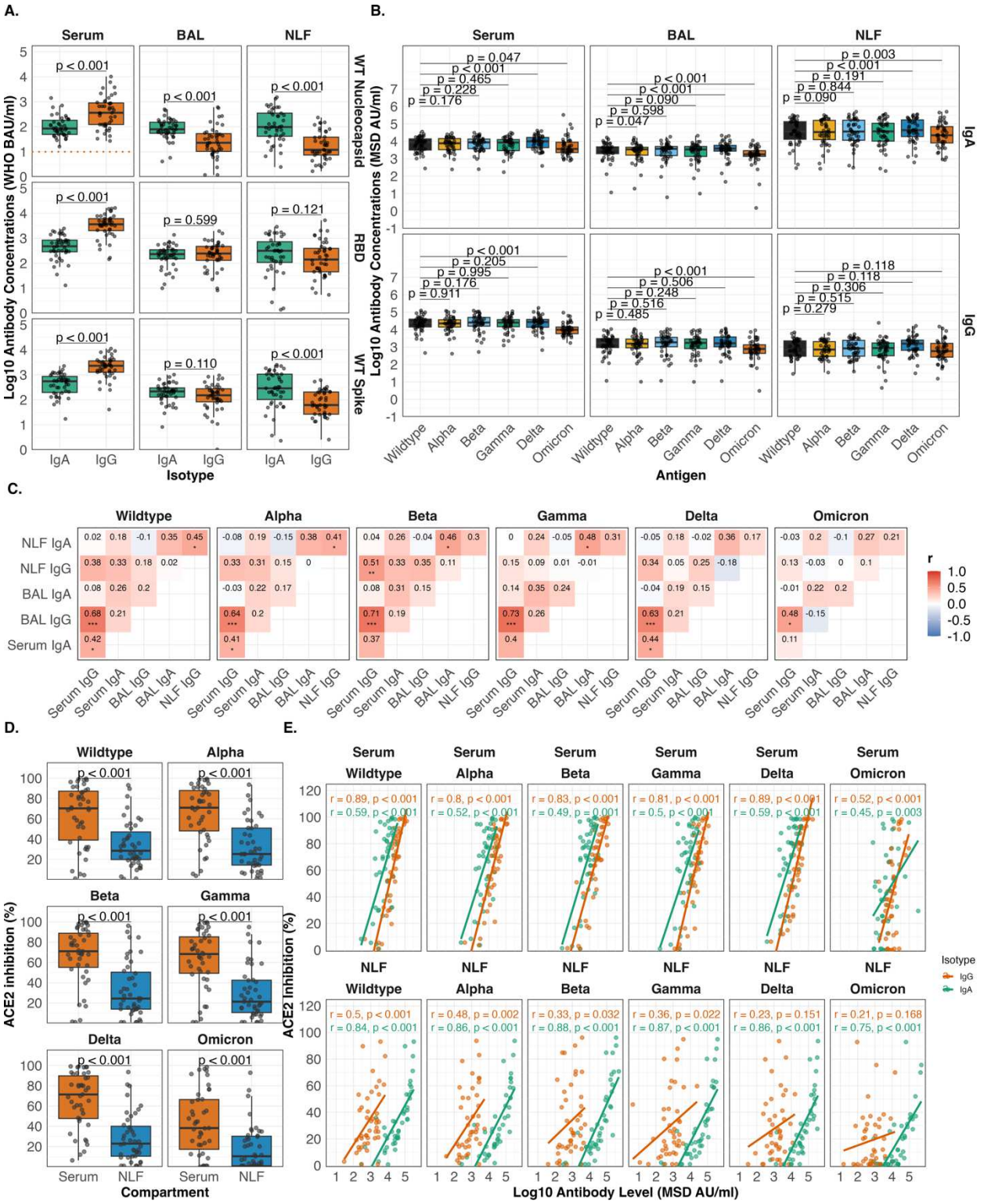


Figure 1 | SARS-CoV-2–specific binding antibody responses in systemic and mucosal compartments.

Serum, bronchoalveolar lavage (BAL), and nasal lining fluid (NLF) from HIV-uninfected adults were analysed for IgG and IgA antibody responses against SARS-CoV-2 Spike wildtype and variants of concern (VOCs), including Alpha, Beta, Delta, Gamma and Omicron. Antibody titres were quantified using a multiplex MSD assay, and ACE2–Spike binding inhibition was measured using a surrogate neutralisation assay. **a,** Box plots comparing WT SARS-CoV-2 Spike-, Receptor Binding Domain (RBD)- and Nucleocapsid-specific IgG and IgA antibody concentrations in serum, BAL, and NLF (n = 41). Antibody concentrations are expressed as WHO binding antibody units (BAU ml^{-1}). Dotted orange line represents cut-off for seropositivity. **b,** Box plots showing the breadth of IgG and IgA antibody responses against SARS-CoV-2 wildtype, Alpha, Beta, Delta, Gamma and Omicron variants in serum, BAL and NLF (n = 43). **c,** Correlogram depicting relationships between IgG and IgA binding antibody titres against wildtype, Beta, Delta and Omicron variants across serum, BAL and NLF (n = 43) samples. Numeric values indicate Spearman's correlation coefficients (r). Asterisks denote statistical significance (*P ≤ 0.05, **P ≤ 0.01, ***P ≤ 0.001). **d,** Box plots showing ACE2–Spike binding inhibition activity (%) in serum and NLF against SARS-CoV-2 wildtype, Alpha, Beta, Delta, Gamma and Omicron variants (n = 43). **e,** Scatter plots showing correlations between ACE2–Spike binding inhibition activity (%) and IgG and IgA antibody titres against SARS-CoV-2 wildtype, Alpha, Beta, Delta, Gamma and Omicron variants in serum and NLF (n = 43). Data in panels **a, b, c** and **e** were log_{10}-transformed for statistical analysis and visualisation. Box plots show the interquartile range (25th–75th percentiles), with the median indicated by a horizontal line. Whiskers extend to values within 1.5× the interquartile range, and points beyond this range represent outliers. Statistical significance was assessed using two-sided Wilcoxon signed-rank tests (**a, b, d**) and Spearman's rank correlation tests (**c, e**); $p < 0.05$ was considered significant. P values were adjusted for multiple comparisons within each figure panel using the Benjamini-Hochberg false discovery rate (FDR) method.

Figure 2.

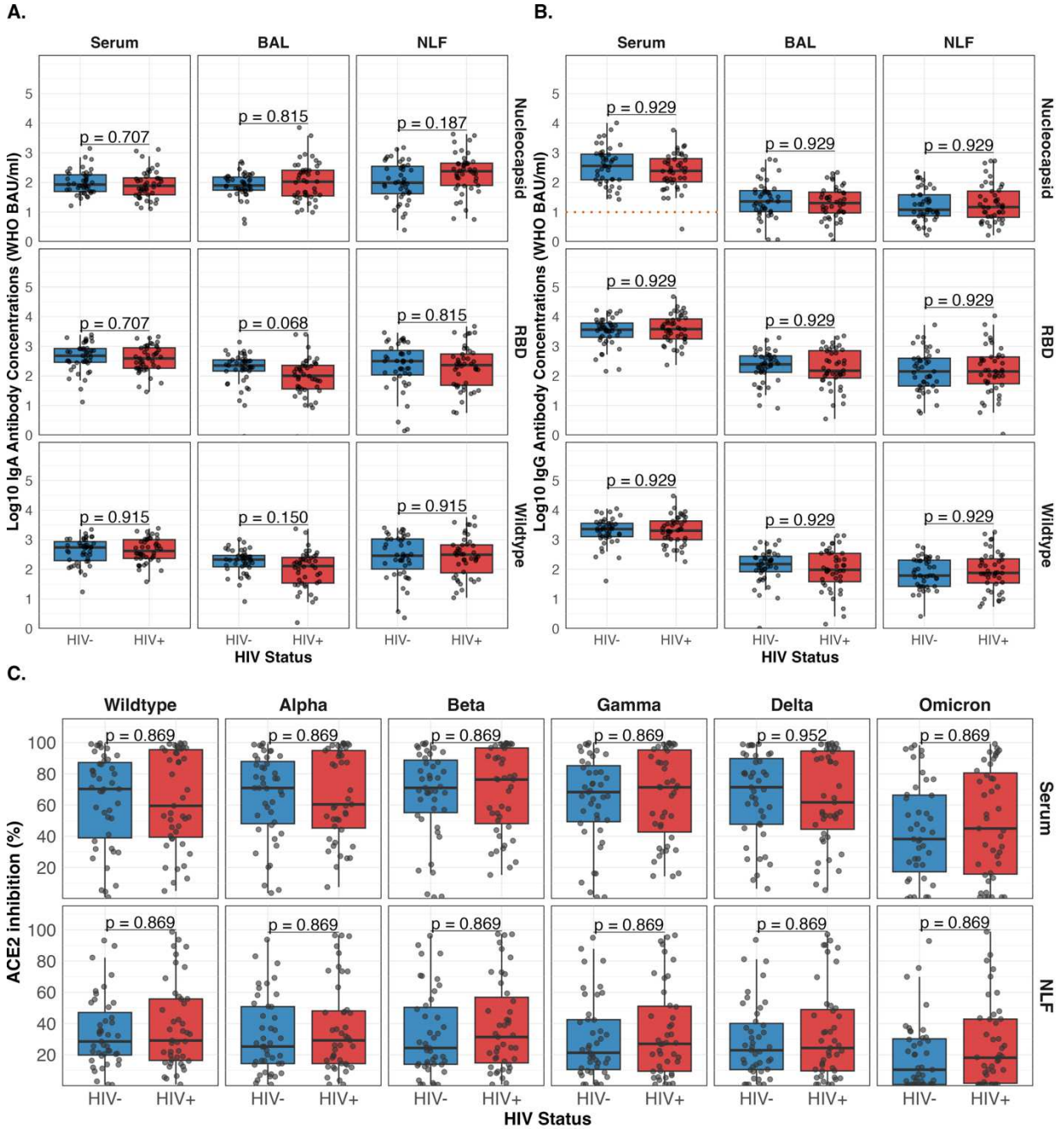


Figure 2 | Comparable SARS-CoV-2–specific antibody responses and ACE2 inhibition between ART-treated people with HIV (PWH) and HIV-uninfected individuals across systemic and mucosal compartments.

SARS-CoV-2 Spike–specific IgG and IgA binding antibody titres and ACE2–Spike binding inhibition activity were compared between PWH and HIV-uninfected individuals in serum, nasal lining fluid (NLF) and bronchoalveolar lavage (BAL) samples against wildtype, Alpha,

Beta, Delta, Gamma and Omicron variants. Antibody titres were quantified using a multiplex MSD assay, and ACE2–Spike binding inhibition was measured using a surrogate neutralisation assay. **a,** Box plots comparing SARS-CoV-2 WT Spike-, RBD- and Nucleocapsid–specific IgA antibody concentrations between PWH and HIV-uninfected individuals. Results are expressed as WHO binding antibody units (BAU ml^{-1}), across systemic and mucosal compartments (HIV-, n = 43, HIV+, n = 45). **b,** Box plots comparing SARS-CoV-2 WT Spike-, RBD- and Nucleocapsid–specific IgG antibody concentrations between PWH and HIV-uninfected individuals. Results are expressed as WHO binding antibody units (BAU ml^{-1}), across systemic and mucosal compartments (HIV-, n = 43, HIV+, n = 45). Dotted orange line represents cut-off for seropositivity. **c**, Box plots comparing ACE2–Spike binding inhibition activity (%) against wildtype and VOCs (Alpha, Beta, Delta, Gamma and Omicron) between PWH and HIV-uninfected individuals in serum and NLF (HIV-, n = 43, HIV+, n = 44). Box plots show the interquartile range (25th–75th percentiles), with the median indicated by the centre line. Whiskers extend to values within 1.5× the interquartile range, and points beyond the whiskers denote outliers. Data in panel **a** was log_{10}-transformed for statistical analysis and visualisation. Statistical significance was assessed using two-sided Wilcoxon signed-rank tests; $p < 0.05$ was considered significant. p values were adjusted for multiple comparisons within each figure panel using the Benjamini-Hochberg false discovery rate (FDR) method.

Figure 3.

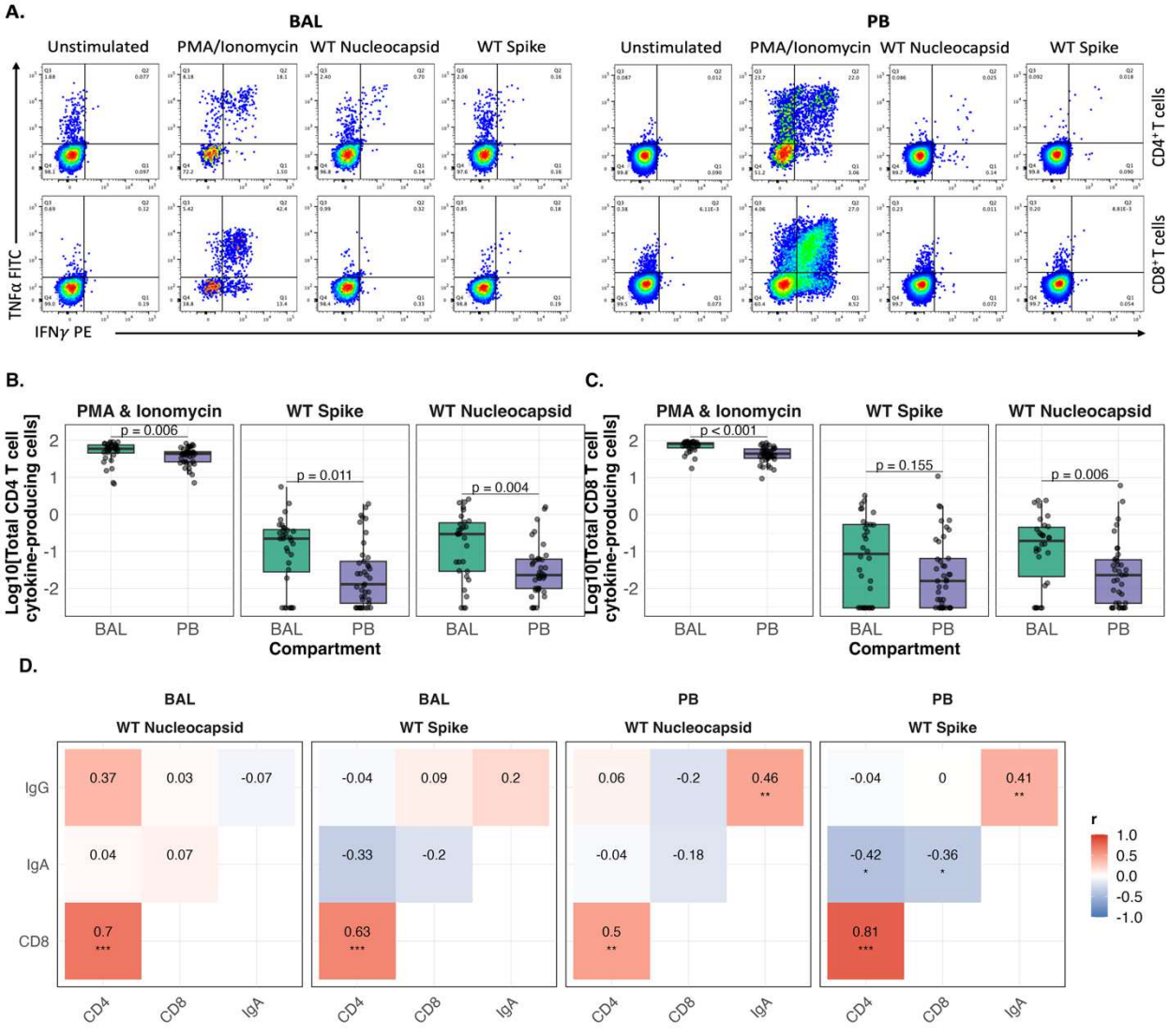


Figure 3 | Detection of SARS-CoV-2–specific T cell responses in systemic and mucosal compartments.

Bronchoalveolar lavage cells (BAL) and peripheral blood (PB) cells collected from HIV-uninfected individuals were stained with fluorochrome-conjugated antibodies to identify total IFN-γ and TNF-α-producing $CD4^+$ and $CD8^+$ T cells following stimulation with SARS-CoV-2 overlapping peptides (WT-spike and Nucleocapsid) and Phorbol 12-myristate 13-acetate and Ionomycin (PMA and Ionomycin). **a,** Representative flow cytometry plots of SARS-CoV-2–specific $CD4^+$ and $CD8^+$ T cell responses in BAL and PB. **b,c** Box plots comparing **b,** $CD4^+$ and **c,** $CD8^+$ T cell responses between BAL and PB following stimulation with PMA/ionomycin

743 (BAL, n = 32; PB, n = 41), SARS-CoV-2 WT Spike (BAL, n = 32; PB, n = 41), and Nucleocapsid
744 (BAL, n = 30; PB, n = 37) peptide pools. **d,** Correlograms depicting the relationships between
745 SARS-CoV-2 WT Spike- and Nucleocapsid-specific $CD4^+$ and $CD8^+$ T cell responses, along with
746 IgG and IgA binding antibody titers (BAL Spike, n = 27; Nucleocapsid, n = 25 and PB Spike, n =
747 36; Nucleocapsid, n = 32). Numeric values indicate Spearman's correlation coefficients (r).
748 Asterisks denote statistical significance (*$p \leq 0.05$, **$p \leq 0.01$, ***$p \leq 0.001$). Data were $\log_{10}$-
749 transformed for statistical analysis and visualisation. Box plots represent the interquartile
750 range (25th–75th percentiles), with the median indicated by the centre line. Whiskers extend
751 to values within 1.5× the interquartile range, and points beyond the whiskers denote outliers.
752 Statistical significance was assessed using two-sided Wilcoxon rank-sum tests (**b,c**) and
753 Spearman's rank correlation tests (**d**); $p < 0.05$ was considered significant.

Figure 4.

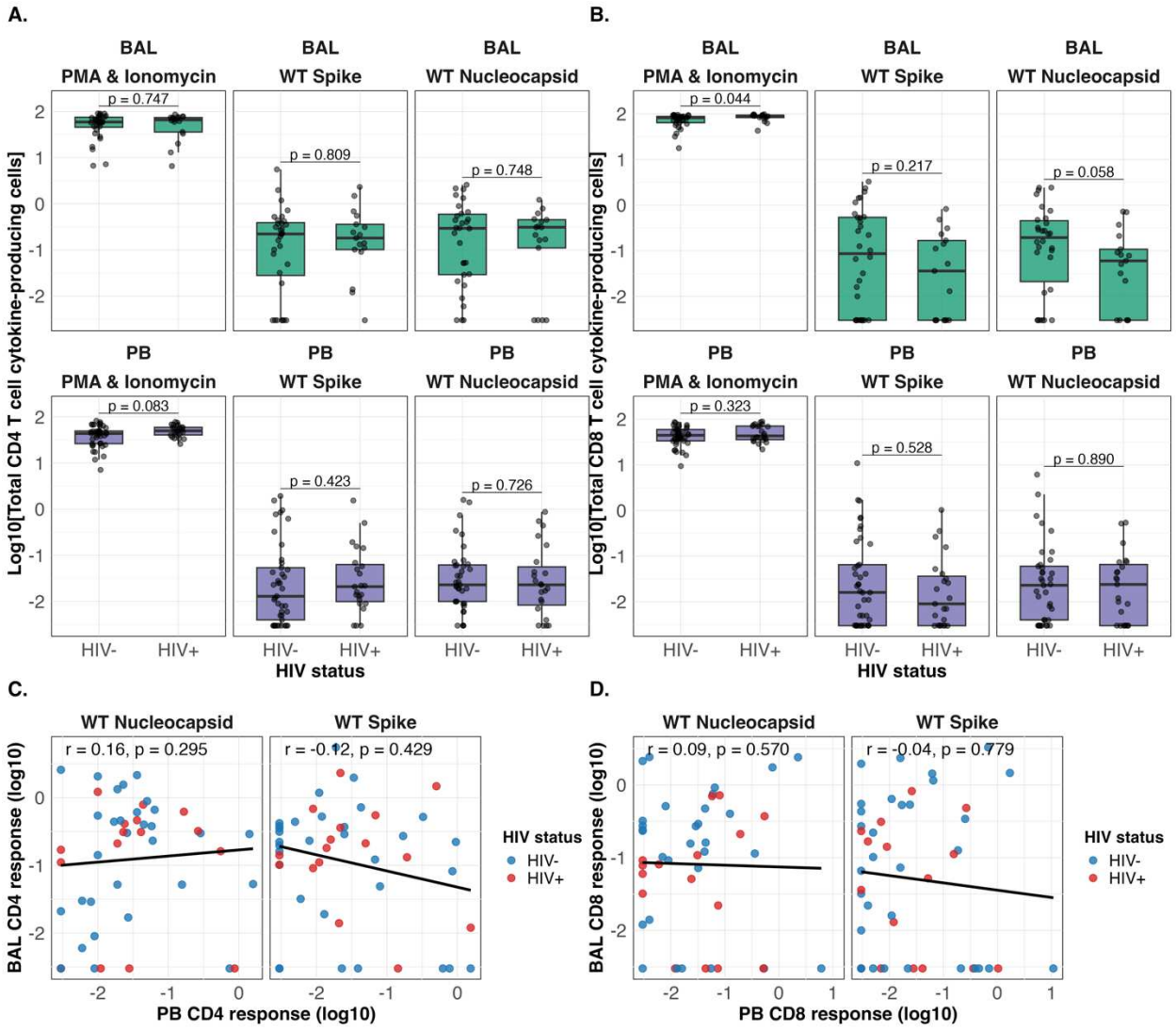


Figure 4 | Comparable SARS-CoV-2–specific T cell responses between ART-treated people with HIV (PWH) and HIV-uninfected individuals across systemic and mucosal compartments.

SARS-CoV-2–specific $CD4^+$ and $CD8^+$ T cell responses were compared between PWH and HIV-uninfected individuals in bronchoalveolar lavage and peripheral blood samples. **a,b,** Box plots comparing **a,** $CD4^+$ and **b,** $CD8^+$ T cell responses between PWH and HIV-uninfected adults following stimulation with PMA/ionomycin, SARS-CoV-2 WT Spike, and Nucleocapsid peptide pools in bronchoalveolar lavage (BAL) and peripheral blood (PB) (HIV-, n = 32; HIV+, n = 17). **c,d,** Correlation plots showing the relationship between BAL and PB SARS-CoV-2 wildtype (WT) spike– and WT nucleocapsid–specific $CD4^+$ and $CD8^+$ T cell responses (n = 48).

Box plots represent the interquartile range (25th–75th percentiles), with the median indicated by the centre line. Whiskers extend to values within 1.5× the interquartile range, and points beyond the whiskers denote outliers. Data in panels **a–b** were $\log_{10}$-transformed for statistical analysis and visualisation. Statistical significance was assessed using two-sided Wilcoxon rank-sum tests (**a,b**) and Spearman's rank correlation tests (**c, d**); $P < 0.05$ was considered significant.

Figure 5.

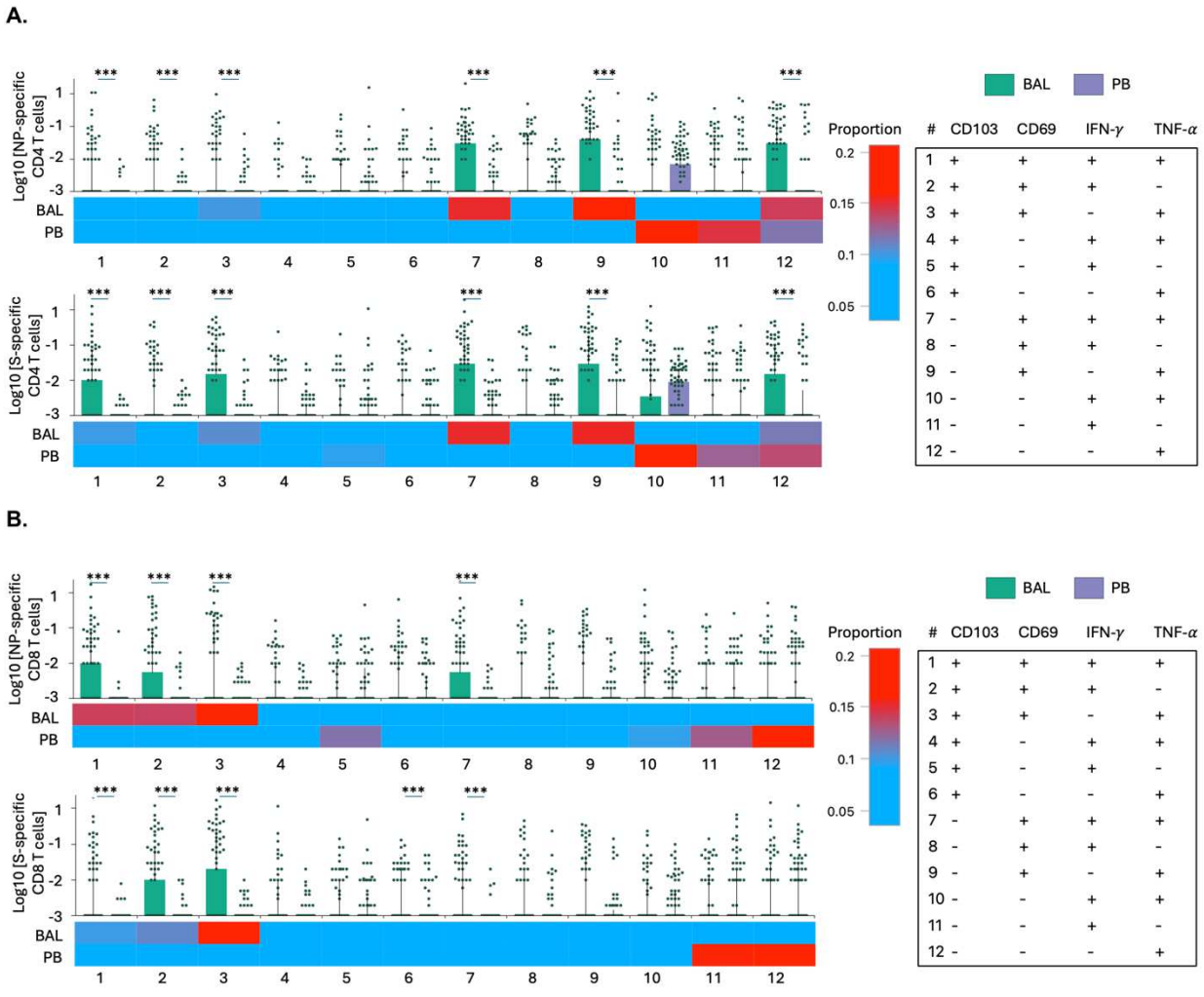


Figure 5 | Phenotypic profiles of SARS-CoV-2–specific T cells across systemic and mucosal compartments.

Scatter plots, bar graphs and heatmaps showing the distribution of WT SARS-CoV-2 Spike- and Nucleocapsid-specific $CD4^+$ and $CD8^+$ T cells in bronchoalveolar lavage samples, pooled across HIV and vaccination status. **a,** WT SARS-CoV-2 Nucleocapsid and Spike-specific $CD4^+$ T cells (S BAL n = 55, PB n = 65; NP BAL n = 54, PB n = 61). **b,** WT SARS-CoV-2 Nucleocapsid and Spike-specific $CD8^+$ T cells (S BAL n = 55, PB n = 65; NP BAL n = 54, PB n = 61). Asterisks denote statistical significance (*p ≤ 0.05, **p ≤ 0.01, ***p ≤ 0.001). Data are presented as median and interquartile range (IQR), with the bar denoting the median. The heatmap denotes the contribution of each specific marker combination to the total response. Statistical analyses

were performed using two-sided Wilcoxon rank-sum tests and Spearman's rank correlation tests; $P < 0.05$ was considered significant.

Supplementary tables

Supplementary Table 1: The table summarises all reagents and antibodies used to generate the data presented in this manuscript.

Reagents used in the experiments shown in this manuscript		
Item	**Manufacturer**	**Product code**
Fetal Bovine Serum	Sigma-Aldrich	F9665
RPMI-1640 Medium (1X) with L Glutamine	Fisher Scientific	12004997
Stemcell Lymphoprep™	Fisher Scientific	07811
Trypan blue	Sigma-Aldrich	T8154
Gibco™ Penicillin-Streptomycin	Thermo Fisher Scientific	15140122
Gibco™ HEPES (1M)	Thermo Fisher Scientific	15630056
Gibco™ Phosphate Buffered Saline (PBS), pH7.2	Thermo Fisher Scientific	11540546
CTL kit (contains-Cryo A, Cryo B, Cryo C)	Cellular Technology Limited (CTL), USA	CTLC-ABC-300
Invitrogen™ LIVE/DEAD™ Fixable Aqua Dead Cell Stain Kit, for 405 nm excitation	Thermo Fisher Scientific	L34957
Invitrogen™ eBioscience™ Fixation/Permeabilization Concentrate	Thermo Fisher Scientific	00-5123-43
Invitrogen™ eBioscience™ Fixation/Permeabilization Diluent	Thermo Fisher Scientific	00-5223-56
Invitrogen™ eBioscience™ Permeabilization Buffer (10X)	Thermo Fisher Scientific	00-8333-56
SULFO-TAG™ Anti-Human IgG detection antibody	Meso Scale Discovery	D21ADF-3
SULFO-TAG™–human ACE2 protein	Meso Scale Discovery	D21ADG-3
MSD Blocker A	Meso Scale Discovery	R93BA-2
GOLD™ Read Buffer B	Meso Scale Discovery	R60AM-2
BD FastImmune™ Co-Stimulatory Antibodies (CD28/CD49d)	BD Biosciences	347690
Brefeldin A (BD GolgiPlug™)	BD Biosciences	555029

Cell Activation Cocktail (without Brefeldin A)	BioLegend	423301
PepTivator SARS-CoV-2 Prot_S Complete	Miltenyi Biotec	130-127-951
PepTivator SARS-CoV-2 Prot_N	Miltenyi Biotec	130-126-698

790

Antibodies used for surface staining of T cells from PBMCs and BAL cells		
Antibody	**Supplier**	**Product code**
APC anti-human CD3 antibody	BioLegend	300312
APC-Cy7 anti-human CD4 antibody	BioLegend	317418
Alexa Fluor® 700 anti-human CD8 antibody	BioLegend	344724
Brilliant Violet 605™ anti-human CD69 antibody	BioLegend	310938
PE-Cy7 anti-human CD103 antibody	BioLegend	350212

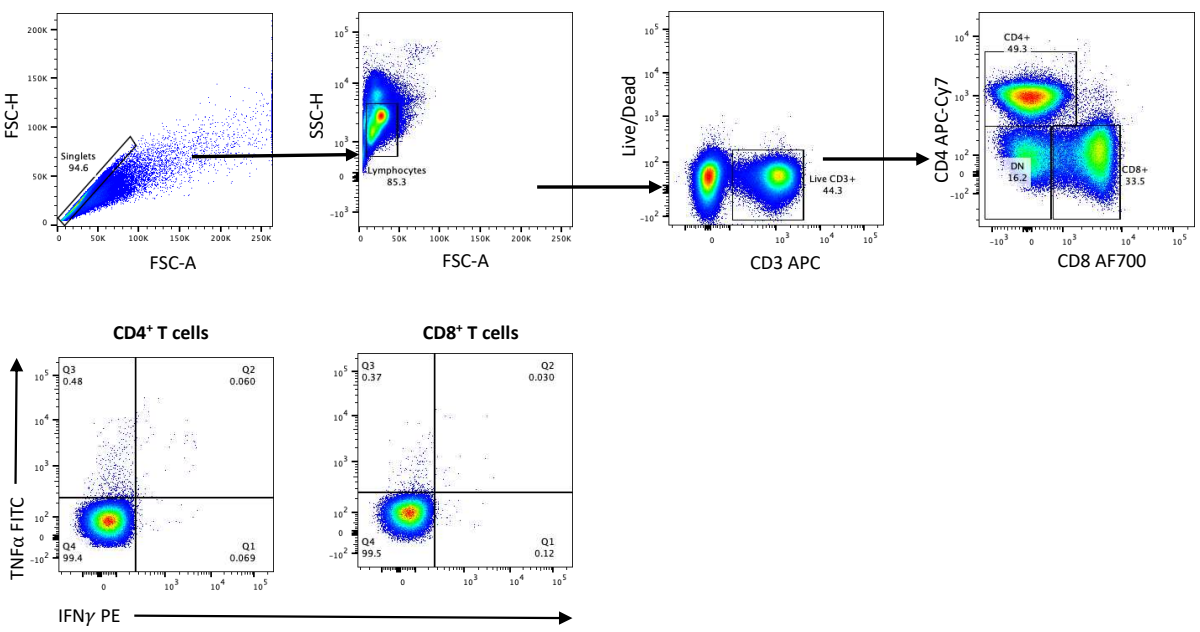
791

Antibodies used for intracellular staining of T cells from PBMCs and BAL cells		
Antibody	**Supplier**	**Product code**
PE anti-human IFN-γ antibody	BioLegend	502509
FITC anti-human TNF-α antibody	BioLegend	502906

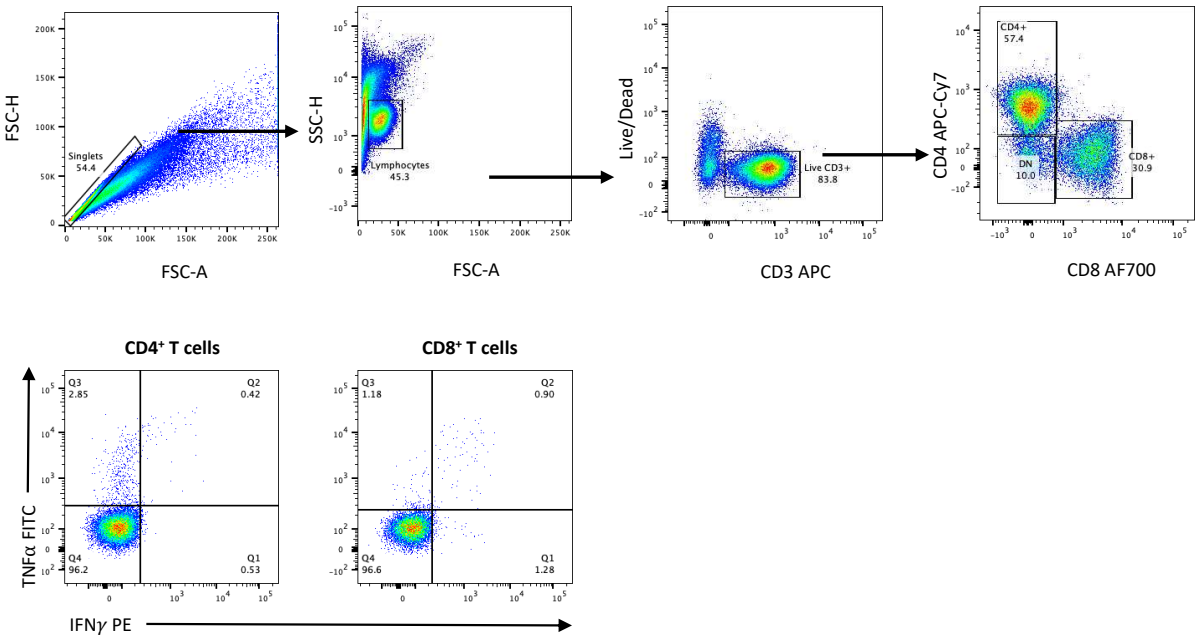
792

Supplementary figures

a. Representative gating strategy for PBMCs



b. Representative gating strategy for BAL



Supplementary Fig. 1 | Flow cytometry gating strategy for systemic and mucosal WT SARS-CoV-2 Spike–specific T cell populations. a, Peripheral blood mononuclear cells (PBMCs) and **b,** bronchoalveolar lavage (BAL) cells were stained with a panel of

fluorochrome-conjugated surface and intracellular antibodies and analysed by flow cytometry. The gating strategy for $CD3^+CD4^+$ and $CD3^+CD8^+$ T cells is shown, including assessment of functional responses (IFN-γ^+, TNF-α^+) following stimulation with WT SARS-CoV-2 Spike peptide.

Supplementary Files

This is a list of supplementary files associated with this preprint. Click to download.

- Supplementaryinfo.pdf